IET Generation, Transmission & Distribution

Research Article

IET Journals
The Institution of Engineering and Technology

Low voltage ride through capability enhancement in a grid-connected wind/fuel cell hybrid system via combined feed-forward and fuzzy logic control

ISSN 1751-8687
Received on 5th January 2019
Revised 11th March 2019
Accepted on 3rd April 2019
E-First on 21st June 2019
doi: 10.1049/iet-gtd.2019.0021
www.ietdl.org

Amit Kumar Roy[1], *Prasenjit Basak*[1], *Gyan Ranjan Biswal*[2] ✉

[1]*Electrical and Instrumentation Engineering Department, Thapar Institute of Engineering and Technology, Patiala, Punjab, India*
[2]*Department of Electrical and Electronics Engineering, Veer Surendra Sai University of Technology, Burla, Odisha, India*
✉ *E-mail: gyanbiswal@gmail.com*

Abstract: Fault ride through (FRT) capability is an essential practice as per the present grid code demands for grid-connected renewable energy-based distributed energy resources. Studies on FRT capability for grid-connected hybrid systems are rarely found. This study considers a wind energy conversion system and a fuel cell system interconnected at a common dc bus. It proposes a new feed-forward-based FRT control scheme for the inverter control where new current references in *dq*-axis frame are derived by tracking the positive sequence power. The newly derived references are fed forward to the input of the current regulator of the voltage source inverter. Second, fuzzy logic-based current controllers are suggested to improve the tracking capability of the current references in the inverter control scheme so as to enhance the FRT capability of the hybrid system as a whole. The proposed feed-forward-fuzzy control scheme for achieving an enhanced FRT capability is compared with the conventional *dq* current control and feed-forward FRT control for various grid voltage sag tests, where the performance of the combined feed-forward-fuzzy control is found better. The validation of the proposed FRT control scheme is performed in MATLAB-Simulink environment.

1 Introduction

With the massive utilisation of renewable energy-based grid-connected (GC) distributed energy resources (DERs), the grid operators have imposed stringent measures and clauses for their grid interconnection. The compliance of IEEE-1547 standard demands a total harmonic distortion of the point of common coupling (PCC) current profile within 5% along with the assurance of grid stability under the event of momentary faults [1]. A bulk DER is required to satisfy the same grid constraints as that of the conventional power plants. Fault ride through (FRT) capability or low-voltage ride through (LVRT) capability emphasises that a large scale DER unit must remain connected or support the utility grid for 0.625 s until a maximum allowable voltage drop at PCC is of 0.15 per unit (PU) [2]. LVRT curves are well defined for the wind generators in the grid codes of Denmark, Germany, Canada etc. The wind generator is expected to stay connected to the grid until the PU voltage levels are above the LVRT curve [3, 4]. An approach for operating multiple DERs in parallel offers the advantage of enhanced system reliability and uninterrupted power at the load end. These DERs may contain sustainable energy sources like photovoltaic (PV) arrays, wind and fuel cell (FC) [5, 6] etc. FC offers appreciable features like modular configuration, eco-friendly, salient operation, and potential to use it as a cogeneration mix for harnessing heat and power both [7–10]. LVRT strategy for permanent magnet synchronous generator (PMSG) has been explored in the previous literature works where two converters namely machine side converter (MSC) and grid side converter (GSC) are controlled by swapping the maximum power point (MPPT) function of the MSC with GSC. While the GSC is made to achieve the ride through control by reactive power injection strategies instead of dc-link voltage control [8, 9, 11, 12].

As per the existing literature, several approaches for the incorporation of FRT in a DFIG-based, PMSG-based, or in a PV-based GC DERs can be found. A general approach is to inject the required reactive power or reactive current via the GC inverter control algorithm as per the magnitude of voltage dip [13–16]. In case of a two-stage configuration PV system, LVRT feature is unified to the system by shifting the MPPT point of the PV panel. This is done by creating a momentarily short circuit across the PV panels during voltage sag condition [17, 18]. Another popular choice to assimilate the LVRT feature in case of DFIG-based wind energy systems is by using additional hardware like a braking chopper or crowbar. This can also be done by capturing the additional energy in the rotor circuit in the form of inertia by using a flywheel or superconducting magnetic energy storage device [19–21]. Nevertheless, the cost of additional hardware, system modification with the addition of new auxiliary devices adds to the system complexity. Another method to include LVRT feature involves the modification of inverter control algorithm where the FRT capability is achieved in GC voltage source inverter (VSI) systems by the generation of flexible current references after the extraction of positive and negative sequence voltages or currents [16, 22]. Flexible control targets are obtained by the GC VSI by controlling the positive, negative, and zero sequence currents simultaneously in [22]. However, the methodology assumes a stiff dc source at the input of VSI and always considers a three-phase, four-wire system which may not be applicable for every distribution system configuration. The incorporation of active power curtailment philosophy is performed in [23] where the power generated from the sustainable power sources is curtailed during a fault condition in order to limit the surge in dc-link voltage. However, this technique is complex and the control algorithm adds computation burden on the inverter control algorithm. Recently, a feed-forward-based control approach along with the conventional PI controller is utilised to mitigate the dc-link fluctuations in PMSG-based wind turbines to provide ride through and frequency support [24].

However, only the dc-link voltage is stabilised while the profile of instantaneous active power is not scrutinised in the study. Nevertheless, this approach is simple and gives credible FRT features. Use of fuzzy logic controllers (FLC) proves to be effective for the control of microgrid system as the amount of nonlinearity in such system is large [25–28]. Fuzzy control is used in [29] for achieving LVRT capability in multiple wind farm using sets of shrinking span membership functions (MFs). However, the discussion on the instantaneous active power profile is not

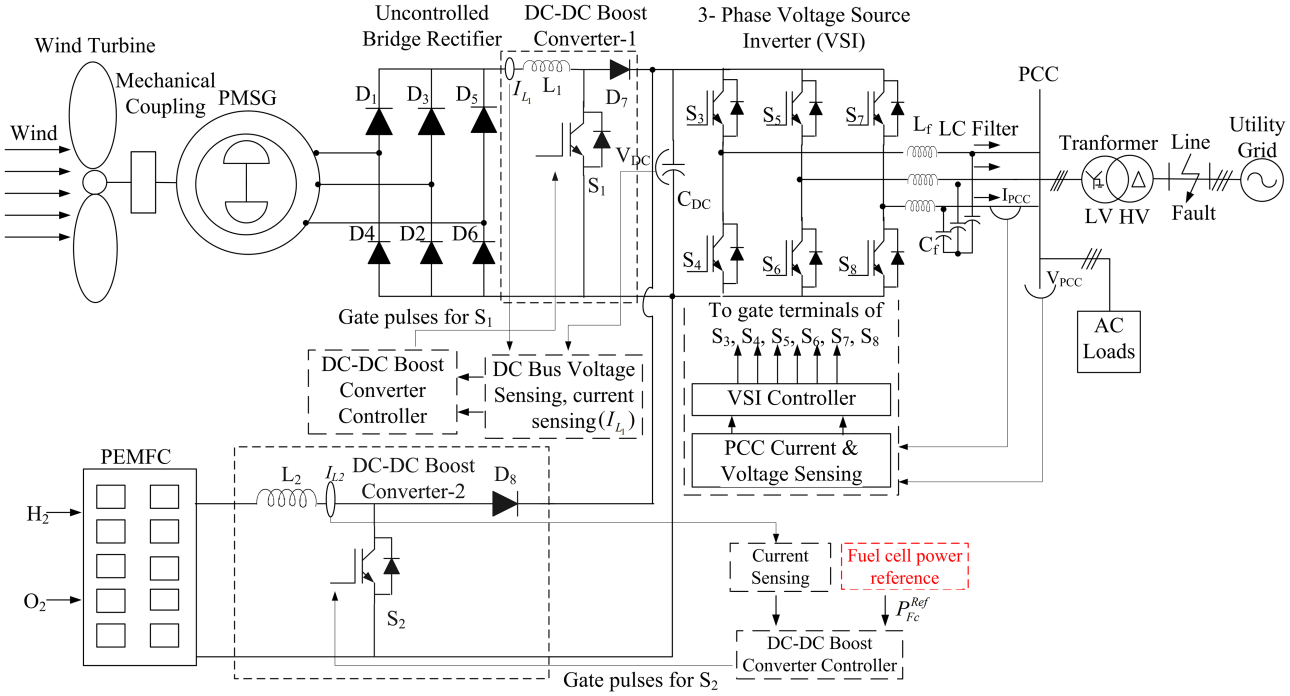

Fig. 1 *Schematic representation of the hybrid sustainable generation system*

performed. In [11], interval type-2 fuzzy control is utilised to achieve enhanced operation for a PMSG wind turbine, but the monitoring of electromagnetic torque of the same is not executed under fault conditions.

From the reviewed literature, it is perceived that the FRT control largely uses a complex control algorithm or uses additional hardware. Fuzzy control is a preferable choice for systems with non-linearities like microgrids. Hence, this paper attempts to contribute towards the enhancement of LVRT capability for a hybrid GC wind/FC system by the following ways

(i). The presented FRT control utilises sequence components to compute the feed-forward current references, which are used in conjunction with the conventional *dq*-current control of the VSI system.
(ii). The proposed FRT control does not use any additional or external devices like series dynamic braking resistor, crowbar circuits, DC link chopper controlled braking resistor, etc. Hence, the use of extra hardware in the system is eliminated.
(iii). This paper proposes the use of FLC_1 and FLC_2 embedded in the control scheme in order to track the newly generated feed-forward current references.

The proposed FRT controller is incorporated for a GC hybrid system consisting of PMSG-based wind generation and a proton exchange membrane FC (PEMFC) system concatenated at a common dc bus whose schematic diagram is as per Fig. 1. This system inherits the technical advantage of rendering continuous power as the PEMFC system may act as back up when power generation from the wind is deficient. In the entire analysis, the power-sharing algorithm between PMSG, PEMFC, loads at the PCC, and the utility grid is not taken into account. Simultaneously, the MPPT functionality of the wind energy conversion system (WECS) under the FRT control phase is not taken into account, as the scope of the paper is to evaluate the FRT studies with the proposed control schemes.

The rest of the paper is organised as follows; the entire hybrid generation system model is briefly discussed in Section 2, the GC hybrid system's behaviour under grid fault and the limitations of the existing FRT control schemes are explicated in Section 3. In Section 4, a thorough discussion on the proposed feed-forward and feed-forward-fuzzy control for rendering the FRT capability is presented. Performance of the proposed FRT controllers is highlighted by considering relevant case studies along with comparative analysis in Section 5. Finally, the conclusions are drawn in Section 6.

2 Hybrid generation system model

A renewable energy-based hybrid generation system considered for the study is depicted as per Fig. 1. The PMSG-based WECS is considered as the primary source of power generation, whereas a PEMFC is added in parallel to the system in order to improve the system redundancy. The system intends to support its local ac loads connected at the PCC and export its excess power during high wind speed to the utility grid. The ac output of the PMSG-WECS is conditioned to dc via an uncontrolled bridge rectifier having diodes D_1–D_6. The dc–dc boost converter-1 with inductor L_1, diode D_7 and controlled insulated gate bipolar transistor (IGBT) switch S_1 performs the function of MPPT. Boost converter-2 with inductor L_2, diode D_8 and controlled IGBT switch S_2 is used to control the FC power as per the desired power reference P_{FC}^{Ref}, such that the power deficit between the WECS and load demand is met. The controlled power conversion from dc to ac is performed by a three-phase VSI having controlled IGBT switches S_3–S_8.

2.1 Modelling of a wind turbine, PMSG, and FC

The mechanical power generated by the wind turbine is given by (1),

$$P_{\mathrm{m}} = \frac{1}{2} C_{\mathrm{p}}(\lambda, \beta) \rho A v^3 \tag{1}$$

where P_m is the mechanical power developed by the wind turbine, ρ is the air density in kilograms per cubic meter, A denotes blades swept area in meter square, v represents wind speed in meter per second, and C_{p} represents power coefficient which is function of tip speed ratio (λ) and pitch angle (β) [8]. In this work a salient pole PMSG is considered, the modelling of stator voltage equations is based on parks transformation which considers synchronously rotating reference frame in the rotor axis expressed by (2) and (3) [11]

$$v_{sd} = L_s \frac{\mathrm{d}i_{sd}}{\mathrm{d}t} + i_{sd} R_s - \omega_e L_s i_{sq} \tag{2}$$

$$v_{sq} = L_s \frac{di_{sq}}{dt} + i_{sq}R_s + \omega_e L_s i_{sd} + \omega_e \varphi \quad (3)$$

where R_s and L_s are resistance and inductance of the PMSG stator winding, respectively; v_{sd}, v_{sq}, i_{sd}, and i_{sq} are the stator voltage and current transformed to dq-reference frame; φ is the magnetic flux; and ω_e is the electrical angular speed.

2.2 Modelling of FC

The PEMFC system is modelled as per the Nernst equation, the internal potential difference between two electrodes (E_{cell}) is given by (4). Here, E_o denotes standard reference potential under standard condition (1-atm and 25°C), taken as 1.229 V. P_{H_2}, P_{O_2}, P_{H_2O} are the corresponding partial pressure of H_2, O_2, and H_2O respectively, R represents the gas constant (8.3143 J/mol K), T stands for temperature of the electrodes in Kelvin, and F represents the Faraday constant (96,487 C/mol). The value of voltage developed at terminals of the FC (V_{cell}) is given as per (5) where $V_{act,cell}$ is the voltage drop due to activation losses, $V_{ohmic,cell}$ is the voltage drop due to ohmic loss and $V_{con,cell}$ is the voltage drop due to concentration loss [9]

$$E_{cell} = \left[E_o + \frac{RT}{2F} \log\left(\frac{P_{H_2} \times P_{O_2}^{1/2}}{P_{H_2O}} \right) \right] \quad (4)$$

$$V_{cell} = E_{cell} - V_{act,cell} - V_{ohmic,cell} - V_{conc,cell} \quad (5)$$

The partial pressures of H_2 and O_2 are related with molar flow of H_2 and O_2 ($q_{H_2}^{in}$, $q_{O_2}^{in}$) and the stack current (I_{stack}) as per (6) [7]

$$\left.\begin{aligned} P_{H_2} &= \frac{1/k_{H_2}}{1 + \tau_{H_2} s}(q_{H_2}^{in} - 2K_r I_{stack}) \\ P_{O_2} &= \frac{1/k_{O_2}}{1 + \tau_{O_2} s}(q_{H_2}^{in} - 2K_r I_{stack}) \end{aligned}\right\} \quad (6)$$

where k_{H_2} is the hydrogen valve molar constant in (kmol/s-atm) whose value is 4.22×10^{-5}, k_{O_2} is the oxygen valve molar constant in (kmol/s-atm) whose value is 2.11×10^{-5}, τ_{H_2} is the hydrogen time constant having value of 3.77 s and τ_{O_2} is the oxygen time constant having value of 6.47 s, K_r is the modelling constant having value of 9.07×10^{-8}.

3 GC VSI behaviour under grid faults

The primary objective of this paper is to investigate the FRT capability of a GC hybrid generation system modelled as per Fig. 1. The main contribution is towards the control of GC-VSI during the faults occurring at high voltage side of the transformer. When fault gets impinged in the system, there is a rapid fall of power at the PCC side. This fall of power may slant to null depending on the severity of the fault, the magnitude of the network impedance, location of the fault etc. While the power generated by the WECS and the PEMFC remains unchanged, the power imbalance between the power generated by DERs and the power at the PCC leads to a rapid surge of power across the dc-link capacitor. This power surge appears instantly in the form of the dc-link voltage surge.

3.1 Dc-link voltage surge and dc-link voltage ripple

The surge in dc-link voltage appears as addition of energy stored by the dc-link capacitor and is accompanied by the presence of voltage ripples. Voltage ripples occur due to the presence of voltage and current unbalance happening because of the injection of negative sequence voltage and current components in the power system. The energy absorbed by the dc-link capacitor due to voltage surge is expressed as per (7) [19]

$$\Delta P_{dc} \cdot \Delta t = \frac{1}{2} C_{dc} (\bar{v}_{dc} + \Delta v_{dc})^2 - \frac{1}{2} C_{dc} \bar{v}_{dc}^2 \quad (7)$$

where ΔP_{dc} is the change in dc-link power, Δt is the transient time, C_{dc} is the dc-link capacitance, $\bar{v}_{dc}$ is the mean value of dc-link voltage, and Δv_{dc} is the surge magnitude of dc-link voltage. The approximate analysis results in the magnitude of dc-link voltage fluctuation as

$$\Delta v_{dc} = \frac{\Delta P_{dc} \cdot \Delta t}{C_{dc} \cdot \bar{v}_{dc}} \quad (8)$$

The dc-link voltage fluctuation is undesirable from the viewpoint of the system's stability. A straight forward approach to remove the fluctuations in dc-link voltage can be achieved by increasing the value of dc-link capacitance. However, this approach is non-feasible as it increases system cost and bulkiness.

3.2 Active and reactive power ripple

The grid codes demand the injection of reactive currents by the inverter during the detection of voltage dip at the utility side for FRT accomplishment. The basic mathematical foundation is based on expressing the instantaneous powers in terms of the positive-negative sequence current and voltage components in a suitable reference frame and to perform appropriate current control functionality. During ideal condition, i.e. in the absence of grid fault, the apparent power delivered by the GC VSI contains only the positive sequence voltage and current components. The same may be expressed in synchronous reference frame (SRF) quantities as

$$s = v_{dq}^p (i_{dq}^p)^* \quad (9)$$

where the subscript 'dq' denotes the quantities in dq-axis frame, prefix 'p' denotes positive sequence quantities, '*' represents the complex conjugate term, v_{dq}^p denotes the PCC voltage in dq frame, i_{dq}^p is the PCC current in dq frame. During the presence of grid unbalance, the instantaneous apparent power can be expressed in positive and negative sequence quantities in the SRF frame as

$$s = (v_{dq}^p e^{j\theta} + v_{dq}^n e^{-j\theta})(i_{dq}^p e^{j\theta} + i_{dq}^n e^{-j\theta})^* \quad (10)$$

where the prefix 'n' denotes negative sequence quantities, operator 'j' means the 90° phase shift in the electrical quantities and θ is the electrical phase angle. The instantaneous active power $P(t)$ and reactive power $Q(t)$ is represented as (11) and (12) [22]

$$P(t) = P_o + P_{c2}\cos(2\omega t) + P_{s2}\sin(2\omega t) \quad (11)$$

$$Q(t) = Q_o + Q_{c2}\cos(2\omega t) + Q_{s2}\sin(2\omega t) \quad (12)$$

The terms P_o, Q_o in (11) and (12) represent the average active and reactive power, P_{c2}, P_{s2}, Q_{c2}, and Q_{s2} represents the second order ripple components in the active and reactive powers, respectively. The conventional approach involves the converted quantities of (11) and (12) in the SRF quantities as per (13)–(18) in order to achieve flexible control strategies

$$P_o = 1.5(v_d^p i_d^p + v_q^p i_q^p + v_d^n i_d^n + v_q^n i_q^p) \quad (13)$$

$$P_{c2} = 1.5(v_d^p i_d^n + v_q^p i_q^n + v_d^n i_d^p + v_q^n i_q^p) \quad (14)$$

$$P_{s2} = 1.5(v_q^n i_d^p - v_d^p i_q^p - v_q^p i_d^n + v_q^p i_q^n) \quad (15)$$

$$Q_o = 1.5(v_q^p i_d^p - v_d^p i_q^p + v_q^n i_d^n - v_d^n i_q^n) \quad (16)$$

$$Q_{c2} = 1.5(v_q^p i_d^n - v_d^p i_q^n + v_q^n i_d^p - v_d^n i_q^p) \quad (17)$$

$$Q_{s2} = 1.5(v_d^p i_d^n + v_q^p i_q^n - v_d^n i_d^p - v_q^n i_q^p) \tag{18}$$

The terms of (13)–(18) can be represented as per the matrix equation given in (19) while the current references are generated as per (20) according to the desired FRT requirement. It is significant to note that the calculation of the inverse matrix of (20) increases the quantum of computational effort of the digital processor used for the inverter control algorithm

$$\begin{bmatrix} P_O \\ Q_O \\ P_{S2} \\ P_{C2} \\ Q_{S2} \\ Q_{C2} \end{bmatrix} = \frac{3}{2} \begin{bmatrix} v_d^p & v_q^p & v_d^n & v_q^n \\ v_q^p & -v_d^p & v_q^n & -v_d^n \\ v_q^n & -v_d^n & -v_q^p & v_d^p \\ v_d^n & v_q^n & v_d^p & v_q^p \\ -v_d^n & -v_q^n & v_d^p & v_q^p \\ v_q^n & -v_d^n & v_q^p & -v_d^p \end{bmatrix} \begin{bmatrix} i_d^p \\ i_q^p \\ i_d^n \\ i_q^n \end{bmatrix} \tag{19}$$

$$\begin{bmatrix} i_d^p \\ i_q^p \\ i_d^n \\ i_q^n \end{bmatrix}^{\text{ref}} = \frac{2}{3} \begin{bmatrix} v_d^p & v_q^p & v_d^n & v_q^n \\ v_q^p & -v_d^p & v_q^n & -v_d^n \\ v_q^n & -v_d^n & -v_q^p & v_d^p \\ v_d^n & v_q^n & v_d^p & v_q^p \\ -v_d^n & -v_q^n & v_d^p & v_q^p \\ v_q^n & -v_d^n & v_q^p & -v_d^p \end{bmatrix}^{-1} \begin{bmatrix} P_O \\ Q_O \\ P_{S2} \\ P_{C2} \\ Q_{S2} \\ Q_{C2} \end{bmatrix} \tag{20}$$

The above equation can be used to extract the current references for achieving various desired flexible control objectives like (i) smoothening of active power ripples, (ii) elimination of reactive power ripples, (iii) elimination of simultaneous active and reactive power ripples, and (iv) injection of balanced grid currents etc.

The approach of obtaining the flexible control objectives in FRT involves a good amount of computations such as referring the three-phase quantities to SRF quantities, extraction of sequence components of corresponding voltages and currents etc. Moreover, the computation of the inverse matrix as per (20) even further complicates the reference current computation process. Another challenge involves around the tracking of the current references. In general, the PI controllers are the widely acceptable controller variant. The reference tracking functionality is performed by four sets of PI controllers as reported in the literature [22]. However, faults are dynamic in nature and occurrences happen for a range of short span. Hence, the smooth tracking of current references in such cases possesses a considerable amount of challenge. Looking specifically to the challenge of computational burden and effective current reference tracking, this paper attempts to eliminate the above limitations by proposing a set of modalities via introducing feed-forward and fuzzy control. The proposed control approach is named as feed-forward-fuzzy control which is elucidated in the next section.

4 Proposed feed-forward-fuzzy control

The idea proposed in the paper to improve the FRT capability especially for a GC hybrid sustainable GC energy systems is based on the concept of elimination of negative sequence current components and tracking the positive sequence active power. The details of feed-forward current reference generation are elaborated below.

4.1 Feed-forward current reference generation

The generation of the feed-forward current reference is based on the fundamentals of power balance between the generated power by the hybrid sustainable sources and power absorbed by the grid. As depicted in Fig. 2, the quantum of power flow is from hybrid generation system to grid, where the sum of power generated by WECS (P_W) and power generated by FC (P_{FC}) is taken as P_{SUS}. This total power is supplied to the dc-link referred as (P_{DC}), meets various losses in the dc–dc converters, goes to the inverter referred as (P_{INV}), LC filter bearing the filter inductance L_f and filter capacitance C_f and eventually transmitted to the utility grid. The power balance between the dc-link capacitor, and power injected to grid (P_{GRID}) neglecting the converter losses is depicted by

$$P_{SUS} = P_{DC} + P_{INV} + P_{GRID} \tag{21}$$

Assuming a lossless condition where the inverter power losses are neglected, (21) can be expressed as

$$P_{SUS} = P_{DC} + P_{GRID} \tag{22}$$

The grid active power can be expressed as the instantaneous summation of sequence powers in positive sequence (P_p), which is further composed of positive sequence voltage (e_p) and positive sequence current (i_p). The negative sequence power (P_n) is composed of negative sequence voltage (e_n) and negative sequence current (i_n) and zero sequence power (P_o) is composed of zero sequence voltage (e_o) and zero sequence current (i_o). This is expressed as

$$P_{SUS} = P_{DC} + 3(P_p + P_n + P_o) \tag{23}$$

$$P_{SUS} = P_{DC} + 3(e_p i_p + e_n i_n + e_o i_o) \tag{24}$$

Since a three-phase, three-wire system is considered, zero sequence quantities are inherently absent. Due to the absence of neutral terminal, the zero-sequence power term is not included in (24).

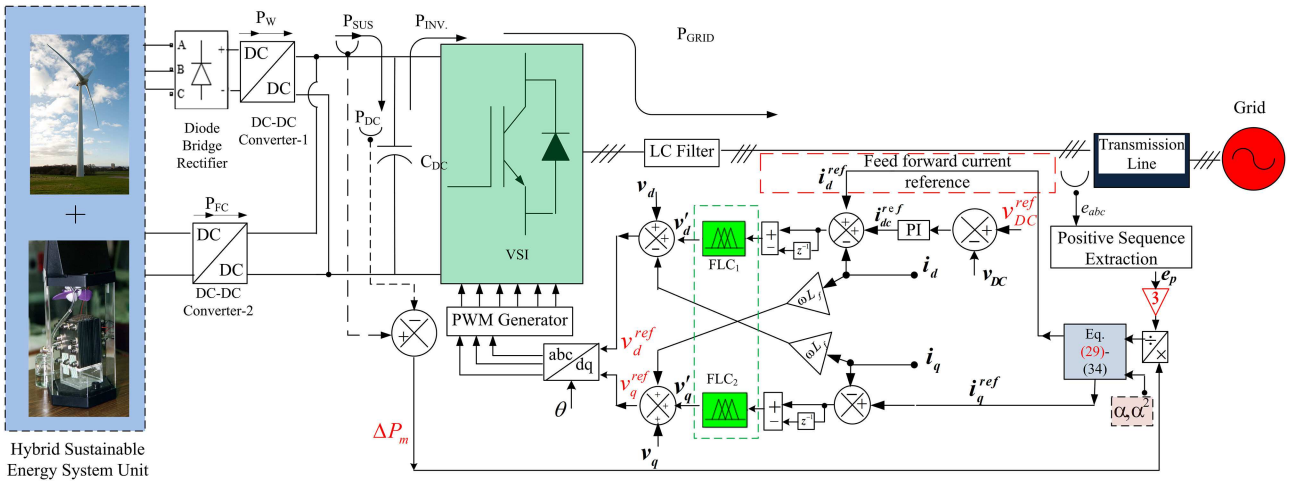

Fig. 2 *Schematic representation of the proposed controller*

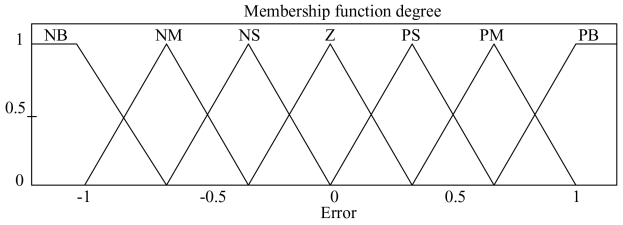

Fig. 3 *MF for input variable 'error $e_1(k)$ and $e_2(k)$'*

During unbalance fault, the presence of negative sequence current and voltage component gives rise to double frequency oscillation in the power delivered to the grid. Thus, in order to incorporate an inverter mechanism which suppresses the oscillating negative sequence power, appropriate current reference needs to be generated. In (24), the negative and zero sequence currents are made null which brings the new expression for P_{SUS} as per (25) and (26). This equation aims to obtain the current references for the grid side inverter such that the negative sequence currents do not appear. The prediction of new current reference (i_p^{ref}) depends on the extraction of positive sequence voltage and its calculation is performed as per (27) and (28). The extraction of e_p is as per the multivariable structure sequence detection scheme algorithm of [13]

$$P_{SUS} = P_{DC} + 3(e_p i_p) \tag{25}$$

Let

$$P_{SUS} - P_{DC} = \Delta Pm \tag{26}$$

substituting (26) in (25) leads to a new expression as (27)

$$3(e_p i_p^{ref}) = \Delta Pm \tag{27}$$

$$i_p^{ref} = \frac{\Delta Pm}{3e_p} \tag{28}$$

The desired positive sequence reference current is obtained as per (28). This current is translated to the instantaneous current phasors '*abc*'. The positive sequence reference currents need the input of sequence factors (α and α^2) which gives phase shift of 120° and 240° to generate the current references as per (29)–(31). The terms of (29)–(31) are complex quantities which cannot be processed by a PI controller. Hence, the modulus operator is applied and the magnitude terms $|i_b^{ref}|$ and $|i_c^{ref}|$ are being used for processing. The reference currents are translated to current reference in the *dq* frame as per (32)

$$i_a^{ref} = \frac{\Delta Pm}{3e_p} \tag{29}$$

$$\begin{aligned} i_b^{ref} &= \alpha^2\left(\frac{\Delta Pm}{3e_p}\right) \\ &= (-0.5 - j0.866)\left(\frac{\Delta Pm}{3e_p}\right) \\ &= \left\{-0.5\left(\frac{\Delta Pm}{3e_p}\right) - j0.866\left(\frac{\Delta Pm}{3e_p}\right)\right\} \end{aligned} \tag{30}$$

$$\begin{aligned} i_c^{ref} &= \alpha\left(\frac{\Delta Pm}{3e_p}\right) \\ &= (-0.5 + j0.866)\left(\frac{\Delta Pm}{3e_p}\right) \\ &= \left\{-0.5\left(\frac{\Delta Pm}{3e_p}\right) + j0.866\left(\frac{\Delta Pm}{3e_p}\right)\right\} \end{aligned} \tag{31}$$

$$\begin{bmatrix} i_d^{ref} \\ i_q^{ref} \end{bmatrix} = \sqrt{\frac{2}{3}}\begin{bmatrix} \cos\theta & \cos(\theta-120^\circ) & \cos(\theta+120^\circ) \\ -\sin\theta & -\sin(\theta-120^\circ) & -\sin(\theta+120^\circ) \end{bmatrix}\begin{bmatrix} |i_a^{ref}| \\ |i_b^{ref}| \\ |i_c^{ref}| \end{bmatrix} \tag{32}$$

$$i_d^{ref} = \sqrt{\frac{2}{3}}\left[\cos\theta \cdot |i_a^{ref}| + \cos(\theta-120^\circ)\cdot|i_b^{ref}| + \cos(\theta+120^\circ)\cdot|i_c^{ref}|\right] \tag{33}$$

$$i_q^{ref} = \sqrt{\frac{2}{3}}\left[-\sin\theta \cdot |i_a^{ref}| - \sin(\theta-120^\circ)\cdot|i_b^{ref}| - \sin(\theta+120^\circ)\cdot|i_c^{ref}|\right] \tag{34}$$

The current reference term obtained in (33) is added to the output of the dc-link PI controller i_{dc}^{ref} obtained after processing the error of reference dc-link voltage v_{DC}^{ref} and actual dc-link voltage v_{DC} to generate the intermediate *d*-axis current as per (35). The proportional and integral gains of the dc-link PI controller are denoted as K_P^V and K_I^V, respectively.

$$i_{dc}^{ref} = K_P^V(v_{DC}^{ref} - v_{DC}) + K_I^V\int(v_{DC}^{ref} - v_{DC})dt \tag{35}$$

The current reference obtained from (33) and (35) is fed forward in the summer block, after which it is subtracted with the actual *d*-axis current (i_d) and is processed further to the inputs of the FLC_1 to generate the intermediate *d*-axis voltage (v_d'). Similarly, the error between *q*-axis current reference i_q^{ref} obtained from (34) and the actual *q*-axis current i_q is pushed to the FLC_2 for obtaining the intermediate *q*-axis voltage term (v_q').

4.2 Fuzzy logic controller design

Since the hybrid generation system has many non-linearities, the reference tracking capability of the PI controller is a challenging aspect. For transient events like faults, the challenge increases manifolds. The paper proposes the use of two FLC controllers FLC_1 and FLC_2 in the VSI control algorithm for tracking the new *d*-axis current reference (i_d^{ref}) and *q*-axis current reference (i_q^{ref}) generated as per (33) and (34). FLC which possess the advantages of easy variable gain generation can work on uncertain system models where the exact mathematical model is unknown. FLC is parameter insensitive and is accompanied with fast convergence [29]. The steps involved in the implementation of FLC consists of fuzzification, design of the fuzzy inference engine and defuzzification, respectively.

4.2.1 Fuzzification: In the fuzzification process, the input signals to the FLC are mapped in the range of [−1 1] and are subsequently assigned MF variables. As the inverter control is based on the sensing of per-unit quantities of voltages and currents, the input variables of FLC are inherently in the range of [−1 1]. Triangular MFs are selected due to the ease of assigning crisp range for different membership variables and these MFs are more sensitive to small signal variations [28]. The input variables for the FLC_1 and FLC_2 are error and change in error, respectively which are shown in Figs. 3 and 4.

The error function for the FLC_1 at the *k*th sample instant is given by $e_1(k) = \left[i_d^{ref}(k) + i_{dc}^{ref}(k)\right] - \left[i_q(k)\right]$ and the change of error denoted by $\Delta e_1(k) = e_1(k) - e_1(k-1)$ is obtained by processing the error through a unit delay block and subtracting the error $e_1(k)$.

Similarly, the error function of the FLC_2 at the *k*th instant is the difference between the reference *q*-axis current and the actual *q*-axis current given by $e_2(k) = i_q^{ref}(k) - i_q(k)$ and the second input of FLC_2 is the change of error denoted by $\Delta e_2(k) = e_2(k) - e_2(k-1)$.

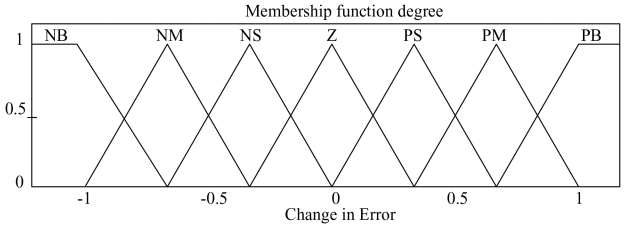

Fig. 4 *MF for input variable 'change in error $\Delta e_1(k)$ and $\Delta e_2(k)$'*

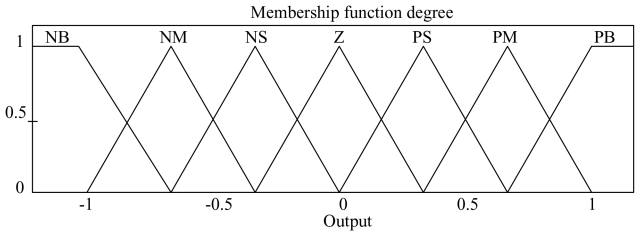

Fig. 5 *MF for output variable v_d' and v_q'*

Table 1 Fuzzy rule base for FLC_1 and FLC_2

Output variables $v_d'$and v_q'		Input variable-2 $\Delta e(k)$						
		NB	NM	NS	ZE	PS	PM	PB
Input variable-1 $e(k)$	NB	NB	NB	NM	NM	NS	ZE	ZE
	NM	NB	NM	NM	NS	NS	ZE	PS
	NS	NM	NM	NS	NS	ZE	PS	PS
	ZE	NM	NS	NS	ZE	PS	PS	PM
	PS	NS	NS	ZE	PS	PS	PM	PM
	PM	NS	ZE	PS	PS	PM	PM	PB
	PB	ZE	PS	PS	PM	PM	PB	PB

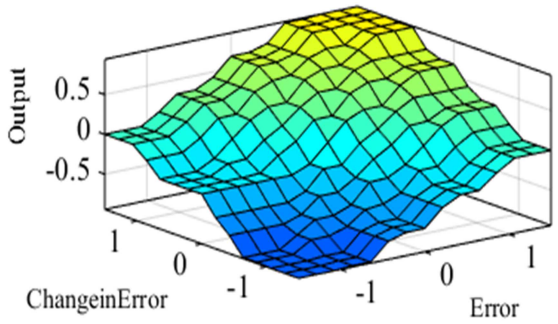

Fig. 6 *Fuzzy rule base surface view*

The output variable of each fuzzy controllers is being represented with the MF as per Fig. 5.

4.2.2 Fuzzy inference engine: The fuzzy inference engine primarily consists of a knowledge base or the rule base which is based on the 'if-then' prepositions. The Mamdani fuzzy inference is used for the design of the proposed FLC_1 and FLC_2 which is based on rules and its related consequents. Crisp output can be fetched after processing the rules, provided overlapping of the neighbouring MFs are ensured [27].

A total of 49 rules is considered for making the correlation between the linguistic variable inputs and outputs of the two fuzzy controllers as presented in Table 1. The linguistic variables are abbreviated as negative big (NB), negative medium (NM), negative small (NS), zero error (ZE), positive small (PS), positive medium (PM), and positive big (PB), respectively. The rules of FLC are selected such that the rise time, overshoot, and settling time of the desired system parameters are minimised as per the required FRT conditions. The surface plot representing the behaviour of the fuzzy rules with the inputs and output variable is shown in Fig. 6.

4.2.3 Defuzzification: The fuzzy controllers have only one output variable which is fetched from the input variable sets. The widely used method for defuzzification is the centre of gravity method. This specific method is selected as it is simple and accurate which calculates the output by calculating the weighted average of the fuzzy functions after the process of the fuzzy rules as per the formula of (36), where, x^* denotes the fuzzy controller's output, x_i is the value of the input variable and $\mu(x_i)$ is the value of the grade of MF [28].

$$x* = \frac{\sum_{i=1}^{n} x_i \mu(x_i)}{\sum_{i=1}^{n} \mu(x_i)} \tag{36}$$

The output voltage terms of FLC_1 and FLC_2 are v_d' and v_q', respectively. These are summed up along with the cross-coupling voltage terms, d-axis voltage v_d and q-axis voltage v_q to give the final dq-axis voltage references v_d^{ref} and v_q^{ref} as per (37) and (38). The phase angle of the PCC voltage θ and the corresponding angular frequency ω provided by the phaselocked loop is also used in the voltage reference generation. The new dq voltage references are translated to abc-references, which are then compared with a PWM bearing a 20-kHz frequency of the carrier signal in order to generate the gate pulses for the VSI. Comparison between the feed-forward FRT control and feed-forward-fuzzy FRT control is presented in Fig. 7

$$v_d^{\text{ref}} = v_d' + v_d - \omega i_q L_{\text{f}} \tag{37}$$

$$v_q^{\text{ref}} = v_q' + v_q + \omega i_d L_{\text{f}} \tag{38}$$

5 Case studies and FRT controller validation

The validation of the proposed feed-forward-fuzzy logic fault ride through (FRT) control is performed by attempting series of test

Feed-forward based FRT control	Feed-forward-fuzzy FRT control
It refers to the inverter current control in order to achieve FRT requirement which is done using the philosophy deliberated in Section 4.1. Here the fuzzy controllers are not used to regulate the current references, instead they are regulated by the conventional PI controllers.	It refers to inverter control done to achieve the FRT requirement by using the philosophy deliberated in Section 4.1 and 4.2 where the new current references for the *d*-axis and *q*-axis are controlled by the fuzzy logic controllers namely FLC_1 and FLC_2.
In the feed-forward based FRT control, the derived current references of Eq. (33) and (34) are controlled in a manner where the current reference i_d^{ref} is fed-forward at the output of the PI controller regulating the dc-link voltage. Further the controller in the inner-loop are PI controllers which regulates the *d*-axis and *q*-axis current reference.	In the feed-forward-fuzzy based FRT control, the derived current references of Eq. (33) and (34) are controlled in a manner where the current reference i_d^{ref} is fed-forward at the output of the PI controller regulating the dc-link voltage. Further the controller in the inner-loop are Fuzzy Logic Controllers (FLC_1 and FLC_2) which regulates the *d*-axis and *q*-axis current reference.
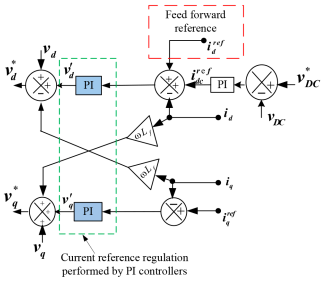	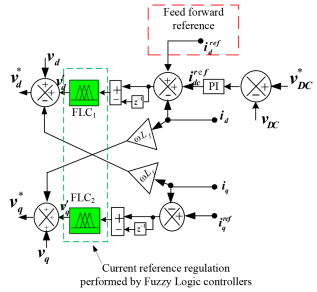
The feed-forward control will render the FRT feature, but will lag performance in terms of effective reference tracking, settling time, over shoot of the dc-link voltage etc. This is due to the inability of the PI controllers to perform effectively on a non-linear system like a grid-connected hybrid generation system as considered in this paper.	The proposed feed-forward-fuzzy-based FRT control performs better since fuzzy logic controller has a better performance while controlling a non-linear system. Hence, to handle the voltage sag problem on a system with high non-linearities like microgrids, the proposed feed-forward-fuzzy based FRT control performs better.

Fig. 7 *Comparison between feed-forward FRT control and feed-forward-fuzzy FRT control*

cases in the MATLAB-Simulink simulation environment. The entire schematic is modelled as per Fig. 1 with the system parameters presented in Table 2. The snippet of the controller part implementation is illustrated in Fig. 8. The case studies involving unbalanced and balanced voltage sag cases viz (a) single phase sag (b) two-phase sag, and (c) three-phase sag are undertaken. Each case is tested for the FRT capability of the hybrid generation using the conventional *dq*-current controller, using only feed-forward FRT control where the current references are completely regulated by the PI controllers and lastly by the proposed combined feed-forward-fuzzy control. In the subsequent sections, the various system parameters for each test cases are portrayed simultaneously on a common axis in order to understand the differences in the individual controller performance with ease.

5.1 System performance under unbalanced sag: one-phase sag

The performance of the hybrid sustainable energy system when a 50% voltage sag at phase-a occurs due to an unbalance fault event at the transmission line is discussed. The PCC voltage of phase-a drops as per Fig. 9*a* during the sag event from 1–1.2 s. The PCC current is shown in Fig. 9*b* for the case when the proposed feed-forward-fuzzy control is used.

It is inferred that the currents are balanced and are limited during the voltage sag span which is due to the effective tracking of the current references by the FLC_1 and FLC_2 unrestricted from negative sequence components. The dc-link voltage profile for three different controllers is presented simultaneously on a common axis as per Fig. 9*c* where the rise and ripples in dc-link voltage profile is prominent for the conventional *dq*-control and feed-forward FRT control, whereas the proposed feed-forward-fuzzy controller outperforms the rest two controllers. The profile of active power delivered to the PCC is as per Fig. 9*d*. In the presented system the rated electrical angular frequency of the instantaneous positive sequence current is 314 rad/s while the negative sequence currents possess an angular frequency of 314 rad/s, which comes to the system during unbalance fault condition. Thus, the resultant angular frequency of the current becomes 314 rad/s−(−314 rad/s) = 628 rad/s, i.e. twice the rated angular frequency. This appears as a form of ripples in the active power profile. The frequency of ripples is such that the instantaneous value of power will be oscillated at a rate of twice the rated angular frequency. Thus, the power ripples possess a frequency of 100 Hz. From Fig. 9*d*, it is established that the proposed feed-forward-fuzzy

Table 2 System Parameters

PMSG wind energy system	
rated power	40 kW
rated speed	314 rad/s
rated torque	126 Nm
base wind speed	12 m/s

PEMFC stack [9]	
power rating	1200-W
DC voltage range	22–50 V
rated voltage	26 V
rated current	46 A
number of cells	48
nominal stack efficiency	46%
operating temperature	55°C
nominal supply pressure of H_2	1.5 Bar
nominal supply pressure of O_2	1 Bar

system electrical parameters	
base voltage (line to line)	415 V
VSI switching frequency	20-kHz

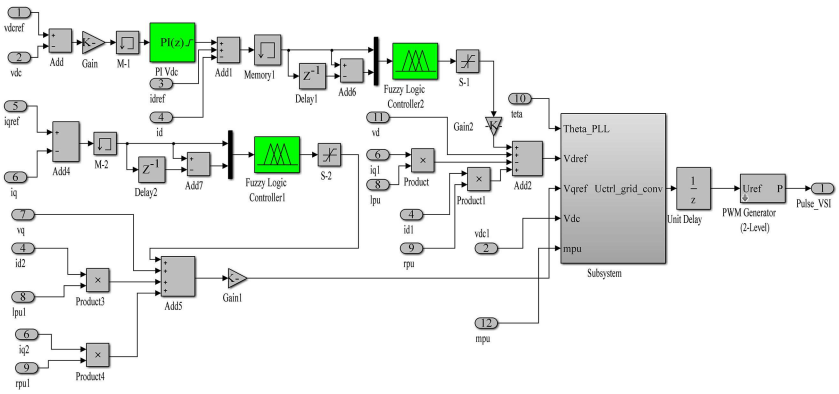

Fig. 8 *Matlab-Simulink implementation of the feed-forward-fuzzy controller*

control achieves a much smoother profile with less power oscillation and power surge. The effectiveness of the proposed feed-forward-fuzzy control over other FRT control method is due to the minimisation of the magnitude of the negative sequence currents as per Fig. 9*e*. Table 3 shows the comparative analysis of various controllers used for the FRT provisions where it is evident that the combined effect of the proposed feed-forward-fuzzy control gives a better FRT behaviour compared to the conventional *dq*- control and with only feed-forward FRT control.

5.2 System performance under unbalanced sag: two-phase sag

In this case, a more stringent condition is applied to test the LVRT efficacy of the proposed feed-forward-fuzzy FRT controller. During a two-phase voltage sag, the magnitude of the voltage dip is much more as compared to a single-phase voltage sag. As observed from Fig. 10*a* dip in phase-a and phase-b voltages are present during the span of 1–1.2 s. The PCC currents are balanced during the faulted span as per Fig. 10*b* due to the proposed feed-forward-fuzzy control. A larger inrush of active power from the DER during two-phase voltage sag leads to a larger surge in the dc-link voltage when no FRT control is applied. While the feed-forward FRT control is unable to mitigate the surge in the dc-link voltage due to the poor regulation of its PI controllers, the proposed feed-forward-fuzzy control FRT control enables a better dc-link voltage profile free from oscillations which is evident as per Fig. 10*c*. Similar behaviour is found in the case of the profile for generated active power where the power oscillation magnitude is much lesser for the proposed feed-forward-fuzzy controller during the faulted span which is as per Fig. 10*d*. While evaluating the negative sequence currents during one-phase sag the tuned values of K_P and K_I of the PI controllers used in the inner current control loop of the feed-forward FRT control could successfully regulate the current reference and reduce the magnitude of negative sequence currents as per Fig. 9*e*. While the same values of K_P and K_I for the PI current regulators were used for the FRT control during two-phase sag, but these gains could not achieve the sufficient amount of current reference regulation so as to quench the negative sequence currents during two-phase sag. In order to achieve a better FRT control during two-phase voltage sag using the feed-forward FRT control, fresh tuning of PI controllers is required. This limitation is overcome by the use of feed-forward fuzzy logic FRT control. It is capable of handling the system non-linearities and provides dynamic current regulation for different voltage sag conditions once the rule base is properly established. The magnitude of negative sequence current for the feed-forward-fuzzy control is less as shown in Fig. 10*e*. A parametric comparison between the existing *dq*-control [30], feed-forward FRT control and the proposed feed-forward-fuzzy FRT control is presented in Table 4.

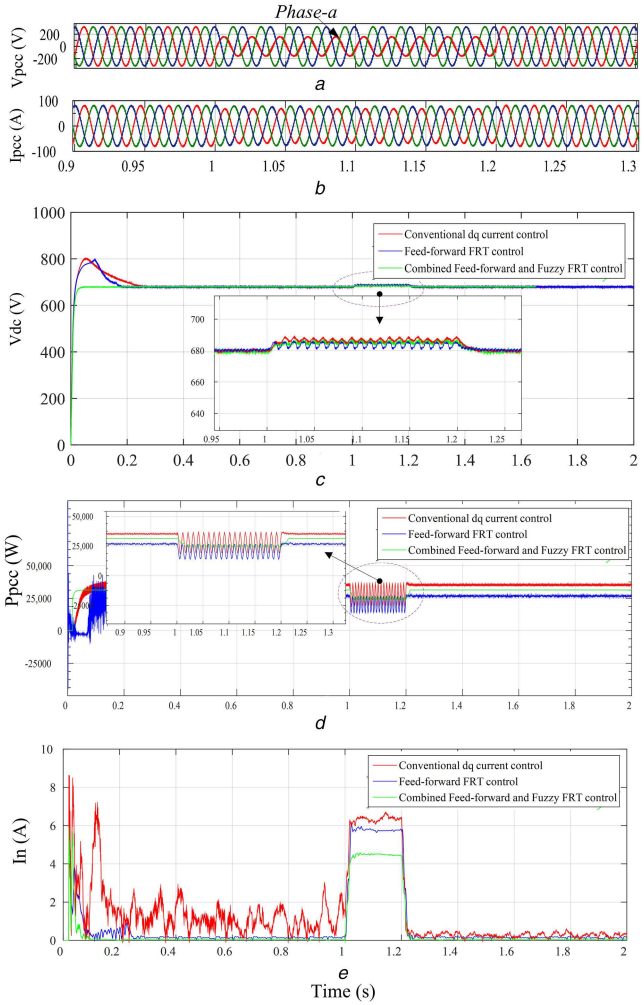

Fig. 9 *Parameters at PCC during one-phase sag*
(a) PCC voltage, ***(b)*** PCC current, ***(c)*** DC link voltage, ***(d)*** Active power delivered, ***(e)*** Negative sequence current

Table 3 Comparative analysis of the FRT control performance for various controllers under 50% voltage sag at phase-a

Parameters	Conventional *dq* control [30]	Feed-forward FRT control	Proposed feed-forward-fuzzy FRT control
dc-link voltage (peak value)	690 V with oscillations	685 V with oscillations	684 V with less oscillations
active power (peak value)	34-kW with oscillations	26-kW with oscillations	25-kW with minimised oscillations
negative sequence current magnitude	7 A	5.9 A	4.2 A

5.3 System performance under balanced Sag: three-phase sag

A balanced three-phase sag does not contain any negative sequence current. Hence the profile of dc-link voltage and active power do not contain any oscillations, but the dc-link voltage surge is present. For validation, equal voltage dip at phase-a, phase-b, and phase-c are created as per Fig. 11*a*. The peak value of dc-link voltage with the proposed feed-forward-fuzzy control is 685 V, while the peak value of 700 and 698 V are obtained for the feed-forward and conventional *dq*-control. Another distinct feature of the proposed control is that the peak overshoot and the settling time is less for the profile of active power as per Fig. 11*d*. The voltage

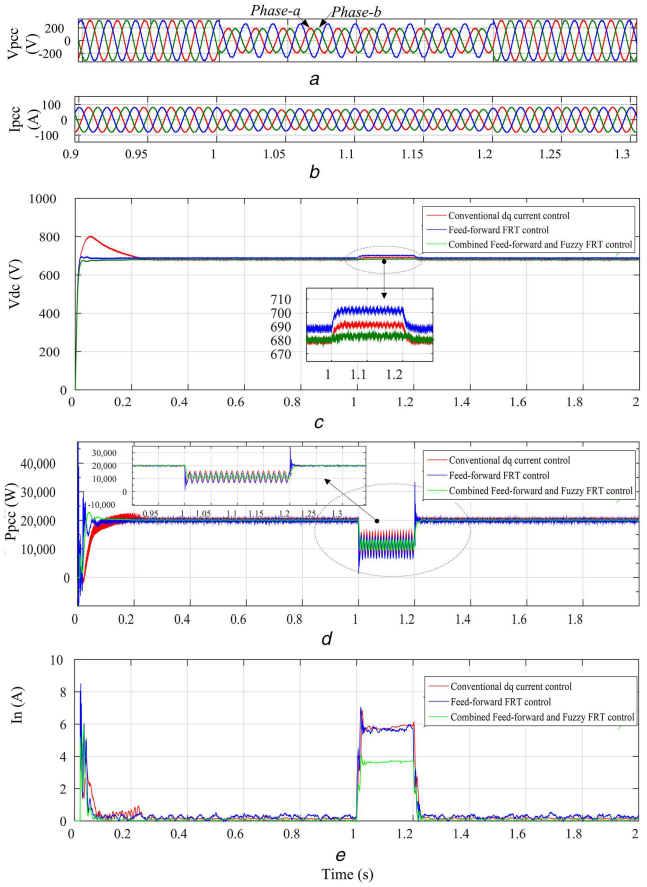

Fig. 10 *Parameters at PCC during 2-phase sag*
(a) PCC voltage, ***(b)*** PCC current, ***(c)*** DC link voltage, ***(d)*** Active power delivered, ***(e)*** Negative sequence current

Table 4 Comparative analysis of the FRT control performance for various controllers under 50% voltage sag at phase-a and phase-b

Parameters	Conventional *dq* control [30]	Feed-forward FRT control	Proposed feed-forward-fuzzy FRT control
dc-link voltage (peak value)	690 V with ripples	700 V with ripples	680 V without any ripples
active power (peak value)	15-kW with ripples	15-kW with ripples	14 kW with less ripples
negative sequence current magnitude	6 A	5.8 A	3.7 A

sag impacts the electromagnetic torque of the PMSG, as the presence of unbalance leads to the generation of torsional oscillations in the PMSG rotor structure. Fig. 12 shows the electromagnetic torque profile of the PMSG. The torque profile of the generator is shown when the PMSG machine is loaded with an electrical load of 3.6 kW. Since the machine runs as a generator, the torque is negative, and corresponding to the electrical power output of 3.6 kW the developed toque is 11.6 Nm. Hence, the torque profile of the machine is registered as −11.6 Nm as per Fig. 12. It is inferred from the result that the electromagnetic torque profile is also better with the use of proposed feed-forward-fuzzy control under voltage sag conditions. Hence the proposed control has not only improvised the dc-link voltage and active power profile, but also the electromagnetic torque profile of the PMSG in the WECS is improved to a great extent.

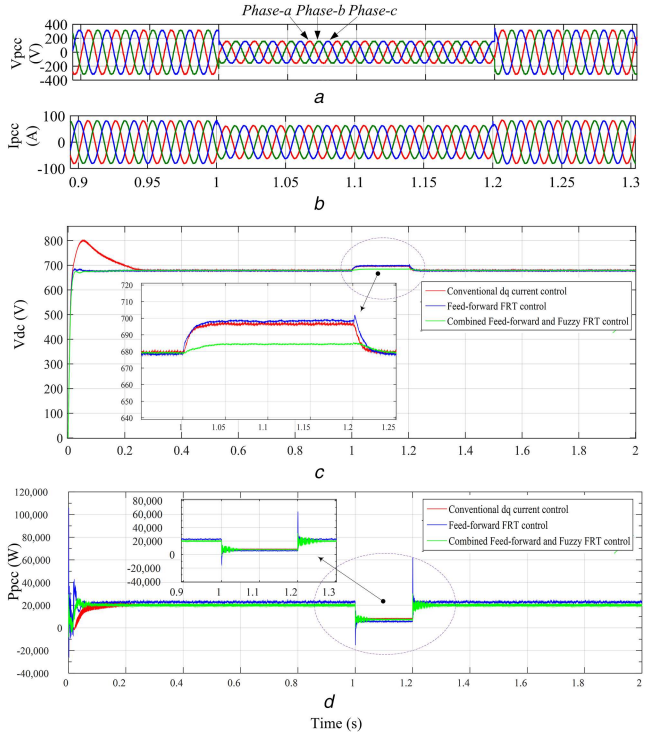

Fig. 11 *Parameters at PCC during 3-phase sag*
(a) PCC voltage, ***(b)*** PCC current, ***(c)*** DC-link voltage, ***(d)*** Active power delivered

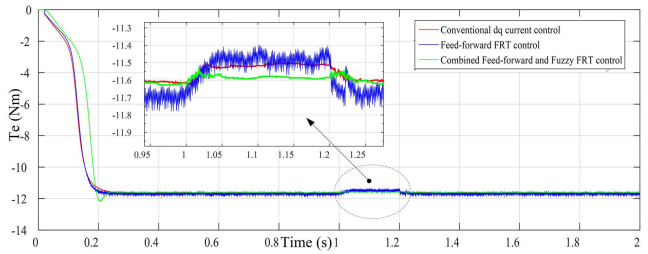

Fig. 12 *Electromagnetic torque of PMSG*

5.4 System performance under variable wind speed and symmetrical fault

A variable wind speed profile is considered to evaluate the performance of the hybrid wind/FC system with the proposed feed-forward-fuzzy control. The system is also subjected to a symmetrical fault for the time span of 1–1.2 s. The wind velocity varies between 10 and 14 m/s as per Fig. 13*a*. The PCC voltage and current profiles are depicted in Figs. 13*b*-*c*, respectively. The overcurrent's are not encountered during the fault span which is due to effective functioning of the feed-forward-fuzzy FRT control algorithm. While the wave-forms of dc-link voltage as per Fig. 13*d* do not show deviations from its reference value during variable wind speed span which indicates the proper power balancing between the generation and demand. Similarly, the active power profile of the PCC as per Fig. 13*e* does not deviate during variable wind speed, this is due to the presence of FC which enables to nullify the power deviations at the PCC even during variable wind speed. The system simultaneously exhibits the FRT feature during the fault span with the proposed feed-forward-fuzzy FRT control strategy.

6 Conclusion

The paper contributes towards the enhancement of the LVRT technology for a GC hybrid sustainable generation system via the design of a new feed-forward FRT control. The proposed feed-forward FRT controller's mathematical model is based on the extraction of a new set of current references such that the surge in the dc-link voltage, ripples in the active power profile and negative sequence current in the system is minimised. Further, the paper

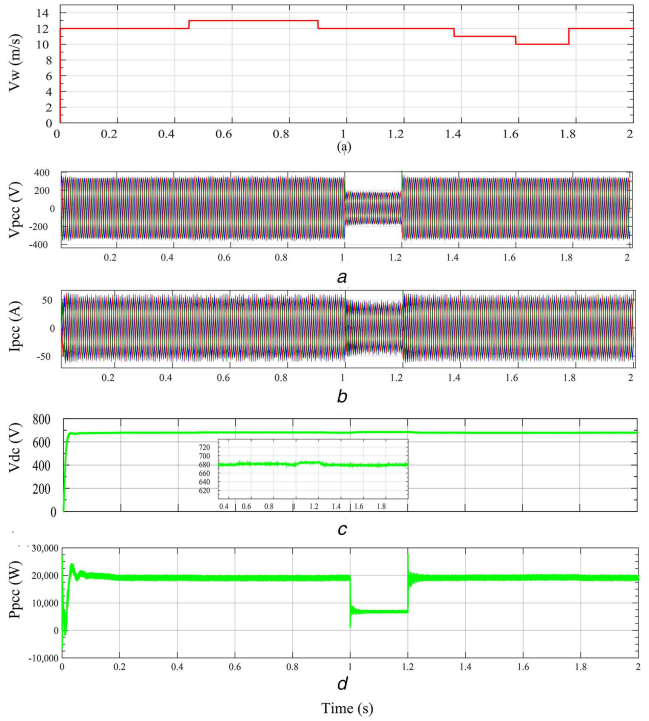

Fig. 13 *Parameters at PCC during variable wind speed and symmetrical fault*
(a) Wind speed V_W ***(b)*** PCC voltage, ***(c)*** PCC current, ***(d)*** DC link voltage, ***(e)*** Active power delivered, ***(e)*** Negative sequence current

improvised the feed-forward FRT scheme with the inclusion of two sets of FLCs to form a feed-forward-fuzzy FRT controller which proved to be a better choice for achieving the FRT capability. The feed-forward-fuzzy control outperformed the conventional *dq*-controller and feed-forward FRT control, which is justified by categorically comparing the system performance during one-phase, two-phase, and three-phase voltage sag. Also, the system's performance during simultaneous wind speed variation and the symmetrical fault is found satisfactory with the proposed control. Alternatively, it can be concluded that the proposed feed-forward-fuzzy control can fulfil the FRT requirement of the considered GC hybrid sustainable generation system in an effectual way. Moreover, a smooth profile of the PMSG electromagnetic torque is registered under voltage sag conditions which prove to be an additional advantage of the proposed feed-forward-fuzzy FRT control scheme.

7 References

[1] IEEE Standard for Interconnection and Interoperability of Distributed Energy Resources with Associated Electric Power Systems Interfaces: 'IEEE Std 1547-2018 (Revision of IEEE Std 1547-2003), pp. 1–138, 6 April 2018

[2] Díez-Maroto, L., Rouco, L., Fernández-Bernal, F., *et al.*: 'Fault ride through capability of round rotor synchronous generators: review, analysis and discussion of European grid code requirements', *Electr. Power Syst. Res.*, 2016, **140**, pp. 27–36

[3] Tsili, M., Papathanassiou, S.: 'A review of grid code technical requirements for wind farms', *IET Renew. Power Gener.*, 2009, **3**, (3), pp. 308–332

[4] Shin, D., Lee, K., Lee, J., *et al.*: 'Implementation of fault ride-through techniques of grid-connected inverter for distributed energy resources with adaptive low-pass notch PLL', *IEEE Trans. Power Electron.*, 2015, **30**, (5), pp. 2859–2871

[5] Shanthi, P., Uma, G., Keerthana, M.S.: 'Effective power transfer scheme for a grid connected hybrid wind/photovoltaic system', *IET Renew. Power Gener.*, 2017, **11**, (7), pp. 1005–1017

[6] Manna, D., Goswami, S.K., Chattopadhyay, P.K.: 'Optimisation of droop coefficients of multiple distributed generators in a micro-grid', *IET Gener. Trans. Distrib.*, 2018, **12**, (18), pp. 4108–4116

[7] Giustiniani, A., Petrone, G., Spagnuolo, G., *et al.*: 'Low-frequency current oscillations and maximum power point tracking in grid-connected fuel-cell-based systems', *IEEE Trans. Ind. Electron.*, 2010, **57**, (6), pp. 2042–2053

[8] Stewart, E.M., Tumilty, R., Fletcher, J., *et al.*: 'Analysis of a distributed grid-connected fuel cell during fault conditions', *IEEE Trans. Power Sys.*, 2010, **25**, (1), pp. 497–505

[9] Wang, C., Nehrir, M.H., Shaw, S.R.: 'Dynamic models and model validation for PEM fuel cells using electrical circuits', *IEEE Trans. Energy Conver.*, 2005, **20**, (2), pp. 442–451
[10] Roy, A.K., Biswal, G.R., Padhy, N.P.: 'An improvized fuel cell system for stand-alone mode application'. 2016 IEEE Power and Energy Society General Meeting (PESGM), Boston, MA, USA, 2016, pp. 1–5
[11] Yassin, H.M., Hanafy, H.H., Hallouda, M.M.: 'Enhancement low-voltage ride through capability of permanent magnet synchronous generator-based wind turbines using interval type-2 fuzzy control', *IET Renew. Power Gener.*, 2016, **10**, (3), pp. 339–348
[12] Nasiri, M., Mohammadi, R.: 'Peak current limitation for grid Side inverter by limited active power in PMSG-based wind turbines during different grid faults', *IEEE Trans. Sustain. Energy*, 2017, **8**, (1), pp. 3–12
[13] Wang, F., Duarte, J.L., Hendrix, M.A.M.: 'Design and analysis of active power control strategies for distributed generation inverters under unbalanced grid faults', *IET Gener. Transm. Distrib.*, 2010, **4**, (8), pp. 905–916
[14] Al-Shetwi, A.Q., Sujod, M.Z., Blaabjerg, F.: 'Low voltage ride-through capability control for single-stage inverter-based grid-connected photovoltaic power plant', *Sol. Energy*, 2018, **159**, pp. 665–681
[15] Tafti, H.D., Maswood, A.I., Konstantinou, G.*, et al.*: 'Low-voltage ride-thorough capability of photovoltaic grid-connected neutral-point-clamped inverters with active/reactive power injection', *IET Renew. Power Gener.*, 2017, **11**, (8), pp. 1182–1190
[16] El Moursi, M.S., Xiao, W., Kirtley, J.L.: 'Fault ride through capability for grid interfacing large scale PV power plants', *IET Gener. Transm. Distrib.*, 2013, **7**, (9), pp. 1027–1036
[17] Afshari, E., Moradi, G.R., Rahimi, R.*, et al.*: 'Control strategy for three-phase grid-connected PV inverters enabling current limitation under unbalanced faults', *IEEE Trans. Ind. Electron.*, 2017, **64**, (11), pp. 8908–8918
[18] Alepuz, S., Calle, A., Busquets-Monge, S.*, et al.*: 'Use of stored energy in PMSG rotor inertia for Low-voltage ride-through in back-to-back NPC converter-based wind power systems', *IEEE Trans. Ind. Electron.*, 2013, **60**, (5), pp. 1787–1796
[19] Yao, J., Zhou, T., Hu, W.*, et al.*: 'Enhanced control for a direct-driven permanent synchronous generator wind-power generation system with flywheel energy storage unit under unbalanced grid fault', *Electric Power Comp. Syst.*, 2015, **43**, (8–10), pp. 982–994
[20] Xiao, X., Yang, R., Chen, X.*, et al.*: 'Enhancing fault ride-through capability of DFIG with modified SMES-FCL and RSC control', *IET Gener. Transm. Distrib.*, 2018, **12**, (1), pp. 258–266
[21] Rashid, G., Ali, M.H.: 'Fault ride through capability improvement of DFIG based wind farm by fuzzy logic controlled parallel resonance fault current limiter', *Electr. Power Syst. Res.*, 2017, **146**, pp. 1–8
[22] Ma, K., Chen, W., Liserre, M.*, et al.*: 'Power controllability of a three phase converter with an unbalanced ac source', *IEEE Trans. Power Electron.*, 2015, **30**, (3), pp. 1591–1604
[23] Sosa, J.L., Castilla, M., Miret, J.*, et al.*: 'Control strategy to maximize the power capability of PV three-phase inverters during voltage sags', *IEEE Trans. Power Electron.*, 2016, **31**, (4), pp. 3314–3323
[24] He, J., Huang, L., Wu, D.*, et al.*: 'Frequency support from PMSG-based wind turbines with reduced DC-link voltage fluctuations', *CES Trans. Electr. Machines Syst.*, 2018, **2**, (3), pp. 296–302
[25] Bhattacharjee, C., Roy, B.K.: 'Fuzzy-supervisory control of a hybrid system to improve contractual grid support with fuzzy proportional–derivative and integral control for power quality improvement', *IET Gener. Transm. Distrib.*, 2018, **12**, (7), pp. 1455–1465
[26] Mohagheghi, S., Venayagamoorthy, G.K., Rajagopalan, S.*, et al.*: 'Hardware implementation of a mamdani fuzzy logic controller for a static compensator in a multimachine power system', *IEEE Trans. Ind. Appl.*, 2009, **45**, (4), pp. 1535–1544
[27] Hannan, M.A., Ghani, Z.A., Mohamed, A.*, et al.*: 'Real-time testing of a fuzzy-logic-controller-based grid-connected photovoltaic inverter system', *IEEE Trans. Ind. Appl.*, 2015, **51**, (6), pp. 4775–4784
[28] Hasanien, H.M., Matar, M.: 'A fuzzy logic controller for autonomous operation of a voltage source converter-based distributed generation system', *IEEE Trans. Smart Grid*, 2015, **6**, (1), pp. 158–165
[29] Mokryani, G., Siano, P., Piccolo, A.*, et al.*: 'Improving fault ride-through capability of variable speed wind turbines in distribution networks', *IEEE Syst. J.*, 2013, **7**, (4), pp. 713–722
[30] Blaabjerg, F., Teodorescu, R., Liserre, M.*, et al.*: 'Overview of control and grid synchronization for distributed power generation systems', *IEEE Trans. Ind. Electron.*, 2006, **53**, (5), pp. 1398–1409